Enhanced Performance in Traveling-Wave Electroabsorption Modulators Based on Undercut-Etching the Active-Region

Yi-Jen Chiu, Tsu-Hsiu Wu, Wen-Chin Cheng, F. J. Lin, and John E. Bowers

***Abstract*—A novel traveling-wave electroabsorption modulator (TWEAM) based on undercut-etching-active-region waveguide (UEAW) is proposed and demonstrated. By selectively wet-etching the InGaAsP from InP to reduce InGaAsP active region, the waveguide can reduce parasitic capacitance with high conductivity in n-InP and p-InP cladding layers. In comparison with conventional ridge-waveguide (RW) TWEAM, 3 dB lower optical-insertion-loss, at least 6 dB higher in radio-frequency-link gain (dc to 40 GHz), and faster electrooptical response (3-dB bandwidth of 25 GHz at 50 Ω-termination for UEAW and 15 GHz for RW) are obtained in UEAW-TWEAM. A 10-Gbs/s operation with low swing voltage of 0.6 V has been achieved in UEAW-TWEAM, a 3.2-dB enhancement over RW-TWEAM. It indicates the tradeoff in designing electroabsorption modulators can be greatly released.**

***Index Terms*—Electroabsorption, high efficiency, high speed, modulator, semiconductor, traveling wave, undercut etching.**

I. Introduction

ELECTROABSORPTION modulators (EAMs) have attracted a lot of interest in the application of optical fiber communication because high speed, high extinction ratio, compact size is possible along with integration with other semiconductor devices, such as semiconductor lasers, optical amplifiers, and passive components. In an optical-fiber link, low insertion loss and high extinction ratio are always the important figures of merits for judging the performance of EAMs. Since semiconductor optical waveguides are generally formed by p-i-n layers, the EAMs' performance is mainly limited by the highly loaded capacitances in the active region causing two tradeoffs in design, 1) between speed and extinction ratio and 2) microwave loss and optical transmission loss [1]–[5]. Designing and fabricating waveguide cores having small widths is, thus, necessary to reduce the parasitic capacitance. Several types of EAMs have been demonstrated for high bandwidth and efficiency. For example, using short waveguides, the high-speed performance is obtained due to the low resistance–capacitance (*RC*)-lump element at the expense of higher drive voltage [4]–[6]. Long EAMs can easily get large ON–OFF ratio, but with reduced speed. Traveling-wave EAMs (TWEAMs) are used to overcome the *RC*-lump limit [2], [3], [7], [8], and achieve large bandwidth and low drive voltage. However, long waveguides still suffer high microwave and optical loss from the thin active region and small waveguide-cores in p-i-n structures, where the widths are typically 2–3 μm. The main factors determining the microwave loss of p-i-n waveguide are from the loaded capacitance and its serially connected resistances on p- and n-layers in terms of equivalent circuit model [9]. Both lowering the loaded capacitance and the resistances of p- and n- layers can result in lower microwave loss. Moreover, high optical loss in such small and long waveguide greatly restricts the electrical–optical signal-link gain [1], [4]. In order to reduce the optical loss in waveguide [10], [11], high-standard and complicated semiconductor processing is needed to get small size and smooth optical waveguides, or increasing optical-mode with periphery coupling structure is used to enhance optical transmission [12]. In this work, a novel method based on selectively undercut-etching-active-region waveguide (UEAW) to reduce the width of active region with low resistance in cladding layers has been proposed and applied to improve the loss and high-speed properties of the TWEAM modulator.

II. Device Fabrication

The microwave circuit structure and semiconductor processing are based on a TWEAM structure [2], [8]. Semiconductor material used for fabrication is grown on a semi-insulated InP wafer by a metal–organic chemical vapor deposition system. Strain-compensated InGaAsP quantum wells (QWs) (ten 12-nm $In_{0.5}Ga_{0.50}As_{0.97}P_{0.03}$ wells and 11 7-nm $In_{0.91}Ga_{0.09}As_{0.37}P_{0.63}$ barriers) sandwiched by the top p-cladding InP layers and the bottom n-cladding InP layers are deposited as the active region (electroabsorption layers) of waveguide. There are two different types of waveguides fabricated in the same wafer; one is the UEAW and the other is a regular ridge-waveguide (RW) served as the control sample. The processing steps are intentionally kept the same except for undercut-etching-active region. The ridges are formed by $CH_4:H_2:Ar$ reactive-ion-etching through the QWs into n-InP layer, where two types of ridges are formed, 6-μm width for UEAW and 2-μm width for RW. A slight wet etching (HBr-based solution) on the sidewalls of both kinds of ridges is subsequently used to get smoother sidewalls. Following that, in UEAW area, a 2-μm-wide active region is defined by

Manuscript received January 12, 2005; revised June 15, 2005. This work was supported by the National Science Council, Taiwan (NSC 93-2215-E-110-018), by MOE Program for Promoting Academic Excellence under Grant 91-E-FA08-1-4 Taiwan, by the Research and Development of Key Super-Wideband Module Technologies for optical fiber communications 92-EC-17-A-07-S1-025 Taiwan, and by the Defense Advanced Research Projects Agency (DARPA)/RFLICS Program USA.

Y.-J. Chiu, T.-H. Wu, W.-C. Cheng, and F. J. Lin are with the Institute of Electro-Optic Engineering, National Sun Yat-Sen University, Kaohsiung 80424, Taiwan, R.O.C. (e-mail: yjchiu@mail.nsysu.edu.tw).

J. E. Bowers is with the Electrical and Computer Engineering Department, University of California at Santa Barbara, Santa Barbara, CA 93106 USA.

Digital Object Identifier 10.1109/LPT.2005.856377

1041-1135/$20.00 © 2005 IEEE

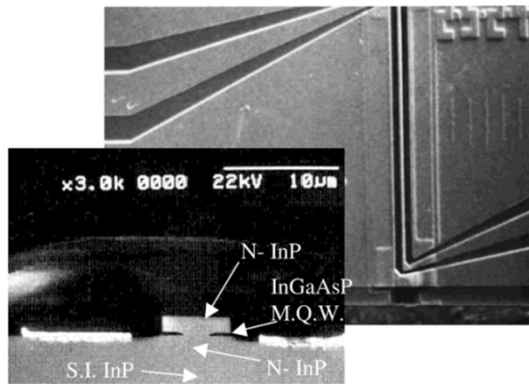

Fig. 1. Top view of undercut-active-region EAM. And the left bottom plot is the cross section of 2-μm-wide waveguide (active region) and the layer structures. A 2-μm active region is made by undercut etching InGaAsP MQWs.

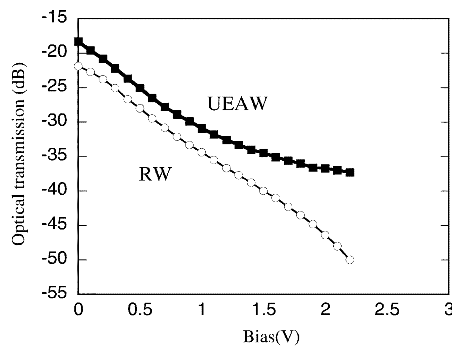

Fig. 2. TE-mode optical transmission with reverse bias for UEAW and RW EAMs. The optical power is set as 0 dBm at wavelength 1550 nm.

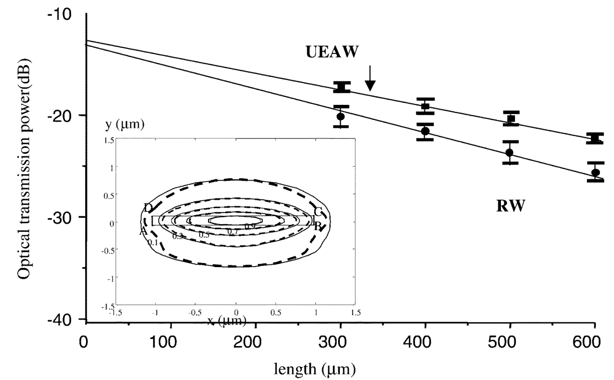

Fig. 3. Optical transmission with different lengths of devices. The insert is the calculated contour plots of the optical modes for UEAW (solid curve) and RW (dashed curve) from 10% to 90% of the highest field intensity. The square region (point A, B, C, and D) is the 2-μm-wide 190-nm-thick active region (InGaAsP QW) for both structures.

selectively undercut-etching the active region (InGaAsP) from n-InP and p-InP layers using a $H_3PO_4 : H_2O_2 :$ DI solution. The p-type (Ti : Pt : Au) and n-type (Ni–AuGe–Ni–Au) metallization are deposited by an e-beam evaporator. PMGI is used for passivating the undercut-etching surface of UEAW and the side wall of RW, planarization and bridging the coplanar waveguide (CPW) interconnected lines. The subsequent measurement on dark current (0.5 V, 20 nA for both structures), photocurrent, and optical transmission on both structures for at least three months shows similar behaviors, indicating the PMGI can passivate the undercut etched side walls. Ti–Au deposition is for the final CPW lines acting as input and output microwave feed lines. Fig. 1 shows the top view (right side) and the waveguide facet (left bottom) of the final device.

III. Measurement, Results, and Discussion

The performance of the two types of EAMs, UEAW and RW, are experimentally compared in three ways: 1) dc optical transmission measurement, 2) high-speed small-signal EO response measurement, and 3) 10-Gb/s large-signal digital-optical-data transmission characterization.

The optical transmission is measured using two fiber-based lenses for input and output optical coupling at an optical wavelength of 1550 nm. Fig. 2 shows transverse-electric (TE) mode optical transmission as a function of bias on 300-μm-long EAMs. About 3–4-dB higher transmission is observed in UEAW than in RW. Similar optical electroabsorption effects for 0–1.5 V are obtained, suggesting that the optical modes of both structures are the same, while the RW type suffers more optical propagation loss in the waveguides. High modulation efficiency of >15 dB/V and large extinction ratio is attributed to the long electroabsorption interaction. As shown in Fig. 3, measuring on different lengths of devices, the optical coupling losses (no AR-coating) are determined to be −12 dB on UEAW and −12.5 dB on RW by extrapolating the transmission curves, confirming the same modes are obtained by both structures. The insert of Fig. 3 plots the calculated optical fields (contour plots, dashed lines for RW and solid lines for UEAW) by the beam propagation method. On the edge of the 2-μm-wide waveguide, the periphery of the UEAWs mode is either buried in the p- and n-layers or surrounding the selective etching surface and the wet-etching surface of only ~190-nm-thick MQW. The calculated optical confinement factors on active region for both structures are 36.5% for UEAW and 35.8% for RW, respectively. Also, the correlation factor between two modes is about 0.99. The main reason causing the lower transmission loss in UEAW is due to the lower scattering loss from selectively wet-etching on the edge of the active region and the buried field in cladding layers [9], [10].

In characterizing the high-speed EO transmission, a high-speed (40 GHz) vector network analyzer incorporating an erbium-doped fiber amplifier (EDFA) and a high-speed photodetector are used to test small-signal EO response. The device is terminated by a 50-Ω resistor at the output port for reducing the microwave reflection. Fig. 4 plots the EO response of 300-μm-long TWEAMs for both types, UEAW and RW. The bias point is set as 0 V. As shown in Fig. 4, the conversion EO efficiency at low frequencies in UEAW is about 6–8 dB higher than in RW confirming the UEAW has approximately 3–4-dB higher dc optical transmission (as shown in Fig. 2). However, the EO efficiency exhibits a significant improvement of 12 dB at frequencies of higher than 30 GHz, indicating the electrical performance at high frequency can be enhanced from UEAW structure. The corresponding 3-dB bandwidth is 25 GHz for UEAW-TWEAM, and 15 GHz for RW-TWEAM. Different bias (from 0 to 0.5 V) and different optical power (from 0 to 8 dBm) are also launched into devices, and similar high-speed EO-responses with level-shifts only are obtained to show no other optical nonlinear effects in the device. Extracted from

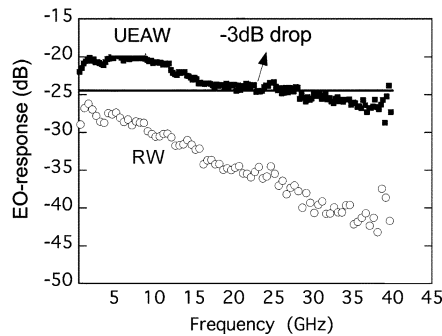

Fig. 4. EO responses of UEAW and RW.

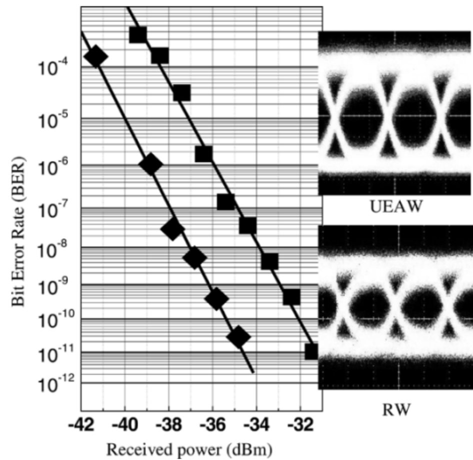

Fig. 5. The 10-Gb/s BERT on UEAW-TWEAM and RW-TWEAM. The insert is the eye diagrams of both structures.

S-parameters, the capacitances are 1.42 nF/m for UEAW and 1.38 nF/m for RW, where the higher capacitance on UEAW is from the parasitic capacitance in the undercut portion. The calculated microwave propagation loss shows that there is at least a 1.8-dB improvement on UEAW than RW at frequencies higher than 30 GHz. It should be noted that UEAW-TWEAM has similar parasitic capacitance as RW-TWEAM; the faster response is still observed implying the wider p-InP and n-InP cladding layers is the main contribution to the lower microwave attenuation inside the waveguide.

A 10-Gb/s data transmission system is also built up to further investigate the properties of TWEAMs of both types under the large electrical signal excitation. A pattern length of $2^{31}-1$ was used by the bit-error-rate-test (BERT) system. The output optical power from a distributed feedback laser was set as 11 dBm with wavelength of 1550 nm. An EDFA at the output of devices was used to amplify the optical signal. A high-speed optical receiver is used as an optical-to-electrical converter. The output swing voltage ($V_{\rm pp}$) from the pattern generator is 0.6 V. As shown in Fig. 5, a clearer and more open eye pattern is observed from UEAW-TWEAM than from RW and the BER measurement shows a large different gap between both types. The sensitivity of -36.2 dBm at BER of 10^{-9} obtained from UEAW-TWEAM is 3.2 dB better than the RW-TWEAM. The power penalty is mainly attributed to the higher optical loss and slower frequency response in RW-type, indicating UEA TWEAM has advantages over RW TWEAM in the overall performance.

IV. Conclusion

Based on the technique of UEAW, a novel type of TWEAM is successfully developed, fabricated, and measured. Reducing the width of active region by selectively wet-etching on InGaAsP from InP results in smooth waveguide, low capacitance, and low resistance in n- and p-cladding layers. As comparing with the conventional RW TWEAM, -3 dB lower for optical transmission loss, and >6 dB higher EO conversion efficiency all over dc to 40 GHz is obtained in UEAW-TWEAM. A 3-dB bandwidth of 25 GHz at 50-Ω termination is obtained in UEAW-TWEAM, which is faster than RW-TWEAM (3-dB bandwidth of 15 GHz). It indicates that the tradeoff between modulation efficiency, high speed, and optical loss in EAMs can be largely reduced by UEAW. A 10-Gb/s operation with $V_{\rm pp}$ swing voltage of 0.6 V has been achieved in 300-μm-long UEAW-TWEAM, while the RW-TWEAM has 3.2-dB power penalty showing this kind of structure has high potential for the application of high-speed and low-loss EAMs.

References

[1] G. L. Li, C. K. Sun, S. A. Pappert, W. X. Chen, and P. K. L. Yu, "Ultrahigh-speed traveling-wave electroabsorption modulator-design and analysis," *IEEE Trans. Microw. Theory Tech.*, pt. 2, vol. 47, no. 7, pp. 1177–1183, Jul. 1999.

[2] C. Z. Zhang, Y.-J. Chiu, P. Abraham, and J. E. Bowers, "25 GHz polarization-insensitive electroabsorption modulators with traveling-wave electrodes," *IEEE Photon. Technol. Lett.*, vol. 11, no. 2, pp. 191–193, Feb. 1999.

[3] S. Irmscher, R. Lewen, and U. Eriksson, "InP-InGaAsP high-speed traveling-wave electroabsorption modulators with integrated termination resistors," *IEEE Photon. Technol. Lett.*, vol. 14, no. 7, pp. 923–925, Jul. 2002.

[4] T. Ido, S. Tanaka, M. Suzuki, M. Koizumi, H. Sano., and H. Inoue, "Ultra-high-speed multiple-quantum-well electro-absorption optical modulators with integrated waveguides," *J. Lightw. Technol.*, vol. 14, no. 9, pp. 2026–2034, Sep. 1996.

[5] K. Wakita, K. Yoshino, I. Kotaka, S. Kondo, and Y. Noguchi, "High speed, high efficiency modulator module with polarization insensitivity and very low chirp," *Electron. Lett.*, vol. 31, no. 23, pp. 2041–2042, Nov. 9, 1995.

[6] R. Weinmann, D. Baums, U. Cebulla, H. Haisch, D. Kaiser, E. Kuhn, E. Lach, K. Satzke, J. Weber, P. Wiedemann, and E. Zielinski, "Polarization-independent and ultrahigh bandwidth electroabsorption modulator in multiquantum-well deep-ridge waveguide technology," *IEEE Photon. Technol. Lett.*, vol. 8, no. 7, pp. 891–893, Jul. 1996.

[7] G. L. Li, S. A. Pappert, P. Mages, C. K. Sun, W. S. C. Chang, and P. K. L. Yu, "High-saturation high-speed traveling-wave InGaAsP-InP electroabsorption modulator," *IEEE Photon. Technol. Lett.*, vol. 13, no. 10, pp. 1076–1078, Oct. 2001.

[8] Y. J. Chiu, H. F. Chou, V. Kaman, P. Abraham, and J. E. Bowers, "High extinction ratio and saturation power traveling-wave electroabsorption modulator," *IEEE Photon. Technol. Lett.*, vol. 14, no. 6, pp. 792–794, Jun. 2002.

[9] K. S. Giboney, M. J. W. Rodwell, and J. E. Bowers, "Traveling-wave photodetector theory," *IEEE Trans. Microw. Theory Tech.*, pt. 2, vol. 45, no. 8, pp. 1310–1319, Aug. 1997.

[10] P. K. Tien, "Light waves in thin films and integrated optics," *Appl. Opt.*, vol. 10, no. 11, pp. 2395–2413, Nov. 1971.

[11] F. Ladouceur and J. D. Love, "Effect of side wall roughness in buried channel waveguides," in *Proc. Inst. Elect. Eng., Optoelectron*, vol. 141, Aug. 1994, pp. 261–266.

[12] Y. L. Zhuang, W. S. C. Chang, and P. K. L. Yu, "Peripheral-coupled-waveguide MQW electroabsorption modulator for near transparency and high spurious free dynamic range RF fiber-optic link," *IEEE Photon. Technol. Lett.*, vol. 16, no. 9, pp. 2033–2035, Sep. 2004.